ORGANIC CHEMISTRY FRONTIERS

RESEARCH ARTICLE

View Article Online
View Journal

Cite this: DOI: 10.1039/d5qo01701g

Chiral π-extended diindenoperylenes featuring dithia[7]helicenes

Georg Berger, Jan Borstelmann, Frank Rominger and Milan Kivala *

Received 17th December 2025,
Accepted 19th January 2026

DOI: 10.1039/d5qo01701g

rsc.li/frontiers-organic

Helically chiral π-expanded diindenoperylenes were synthesized and their chiroptical properties were characterized. The enantiopure synthesis of the perylene framework was achieved by two-fold Yamamoto coupling of π-expanded dibromofluoranthenes, each comprising one dithia[7]helicene unit. Oxidation of the thiophene units to the corresponding sulfones allowed late-stage modification of the chiroptical and electrochemical properties.

Introduction

The synthesis of non-planar, chiral polycyclic aromatic hydrocarbons (PAHs) and nanographenes has sparked widespread interest due to their unique optoelectronic and physical properties.[1–7] Potential applications include spin-selective electron transport[4,8] as well as circularly polarized light (CPL) detection[9] and emission.[10] CPL emitters in the near-infrared region are of particular interest, as, compared to visible light, near-infrared radiation is less absorbed in biological tissues and optical fibres, allowing deeper tissue penetration and far-reaching signal transfer, which are crucial for novel technological and bioimaging applications.[11]

Helicenes are a class of inherently chiral PAHs, where non-planarity is achieved through steric strain preventing a planar geometry.[3,12] The inherent chirality of their π-system makes helicenes useful building blocks for chiral optical and electronic materials. [4]Helicene is considered the smallest helicene. It is only slightly helical due to the steric interactions of the hydrogen atoms in the *bay* region, and the two enantiomeric forms rapidly interconvert through a C_{2v} symmetric, planar transition state.[13] The barrier of racemization increases with the length of the helicene and, for example, enantiomers of [5]helicene are isolable but racemize within days at room temperature (rt),[14] while [6]helicene is considered configurationally stable under ambient conditions.[15]

Examples of helicenes comprising perylene and related polycyclic units are shown in Fig. 1. The [6]helicene **1** recently synthesized by Nuckolls and coworkers features two perylene diimide units at its termini (Fig. 1A). Interactions of the π-systems of both perylene diimide units were demonstrated and attributed to their spatial proximity.[16] Regarding its chiroptical properties, compound **1** exhibits an absorption maximum of $\lambda_{max,abs}$ = 516 nm and a dissymmetry factor g_{abs} = 1.5 × 10^{-3}. In compound **2**, recently synthesized by Wang and coworkers,[17] a perylene unit is embedded in the center of two [6]helicenes, offering an outstanding fluorescence quantum yield of 93% ($\lambda_{abs,max}$ = 538 nm, $\lambda_{em,max}$ = 562 nm)

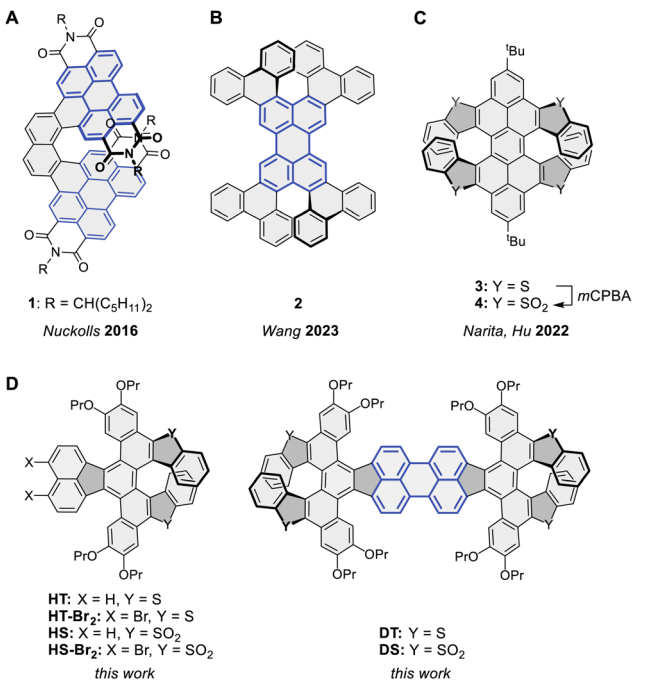

Fig. 1 Examples of configurationally stable π-extended helicenes. (A) [6]Helicene featuring two perylene diimide units.[16] (B) π-Extended perylene comprising two [6]helicene units.[17] (C) Peropyrene-based X-type double dithia[7]helicene and disulfone[7]helicene, demonstrating post-modification of thiophene units.[18] (D) Diindenoperylene-embedded double dithia[7]helicene. Perylene units have been highlighted in blue color. *m*CPBA = *m*-chloroperoxybenzoic acid; Pr = *n*-propyl.

Organisch-Chemisches Institut, Universität Heidelberg, Im Neuenheimer Feld 270, 69120 Heidelberg, Germany. E-mail: milan.kivala@oci.uni-heidelberg.de

and a dissymmetry factor of g_{abs} = 7.0 × 10^{-3} at 360 nm. Compound **3** comprises a peropyrene unit as the centerpiece of an X-type double [7]helicene, with each [7]helicene unit featuring two thiophene units. In compound **4**, these thiophene units were oxidized to the respective sulfones, demonstrating late-stage tuning of the structural and optoelectronic properties.[18] Further noteworthy examples include a perylene-comprising double [5]helicene by Mastalerz and coworkers,[19] showing excellent fluorescence quantum yields of 70% ($\lambda_{abs,max}$ = 488 nm, $\lambda_{em,max}$ = 526 nm), and heptagon-embedded saddle-shaped nanographenes featuring thia[6]helicene units by Hu, Chen, and coworkers,[20] further exemplifying the utility of oxidative late-stage functionalization of the thiophene units.

In this work, we aimed to embed a diindenoperylene between two dithia[7]helicenes, unifying the appealing optoelectronic properties of diindenoperylene[21–23] with the chirality provided by the helicenes and the potential of the thiophene units for late-stage modification[18,24–27] to enable tailored chiroptical characteristics.

Results and discussion

Synthesis

As shown in Fig. 2, the synthesis started from diarylnaphthylenecyclopentadienones **5** and **6**, which were obtained from commercially available methyl 2-(3,4-dihydroxyphenyl)acetate using established methodology (see the SI).[28] A Diels–Alder reaction with bis(benzothiophen-3-yl)ethyne[29] (**7**) yielded the precursors **8** and **9**. Subsequent oxidative cyclization using 2,3-dichloro-5,6-dicyano-1,4-benzoquinone (DDQ) and trifluoromethanesulfonic acid (TfOH) yielded dithia[7]helicenes *rac*-**HT** and *rac*-**HT-Br$_2$**. While an oxidative dimerization of *rac*-**HT** was not achieved, a reductive Yamamoto dimerization of *rac*-**HT-Br$_2$** yielded an inseparable mixture of stereoisomers. Therefore, the two enantiomers of **HT-Br$_2$** were separated by chiral HPLC (for details, see the SI). The subsequent Yamamoto coupling allowed dimerization to the enantiopure double dithia[7]helicenes (*P*,*P*)-**DT** (76%) and (*M*,*M*)-**DT** (81%) under mild conditions, avoiding racemization.

Thiahelicenes *rac*-**HT-Br$_2$** and *rac*-**HT** were oxidized with *m*-chloroperoxybenzoic acid (*m*CPBA) to the corresponding *S*,*S*,*S*′,*S*′-tetroxides *rac*-**HS-Br$_2$** (49%) and *rac*-**HS** (43%).[18] The subsequent Yamamoto dimerization employing *rac*-**HS-Br$_2$** yielded double [7]helicenedisulfone **DS** as an inseparable mixture of diastereomers, albeit in a low yield (14%). To avoid the low-yielding Yamamoto dimerization of **HS-Br$_2$**, double [7]helicenedisulfones (*P*,*P*)/(*M*,*M*)-**DS** were synthesized by the oxidation of (*P*,*P*)/(*M*,*M*)-**DT** with *m*CPBA in yields of 35% and 23%, respectively. For reference, enantiopure (*P*)/(*M*)-**HS** were obtained by oxidation of the respective enantiopure (*P*)/(*M*)-**HT**.

Structure and aromaticity

Single crystals of racemic helicenes **HT**, suitable for X-ray diffraction analysis, were obtained (gas phase diffusion from $CDCl_3$/MeOH), **HT-Br$_2$** (gas phase diffusion, 1,2-dichloroethane/MeCN) and **HS-Br$_2$** (gas phase diffusion, *o*-dichlorobenzene/MeOH) (Fig. 3A and Table 1). The impact of the oxidation of the thiophene units can be observed by comparison of **HT-Br$_2$** with **HS-Br$_2$**. The most notable changes concern the bond lengths in the thiophene unit. The average C–S bond length increases by 0.05 Å, while the C–C bond length in the 5-membered ring opposite to the sulfur atom increases by 0.05 Å. Both changes can be explained through the loss of aromaticity in the thiophene ring upon oxidation, as indicated by the HOMA[30,31] indices and $NICS(1)_{zz,avg}$ values (GIAO[32–38]-CAM-B3LYP[39]/D3BJ[40]/def2-TZVP[41,42]/SMD(CH_2Cl_2)[43])[44] (Table 1 and Fig. 3B). The increased helical pitch may result from the increased bond lengths. The steric demand of the sulfone oxygen atoms should not directly influence the geometric properties of the helicene unit due to their considerable distance. Apart from the thiophene ring, **DT** and **DS** exhibit comparable aromaticity with rings A, A′, D, and D′ of the helicene subunits being highly aromatic (Fig. 3B). In the diindenoperylene unit, HOMA and $NICS(1)_{zz,avg}$ values indicate the low aromaticity of the 5-membered rings (F) and the central 6-membered ring (H), while the other rings (E, G, G′) are indicated as aromatic.

The strongly helical structure and considerable spatial overlap between the terminal benzene rings suggest configura-

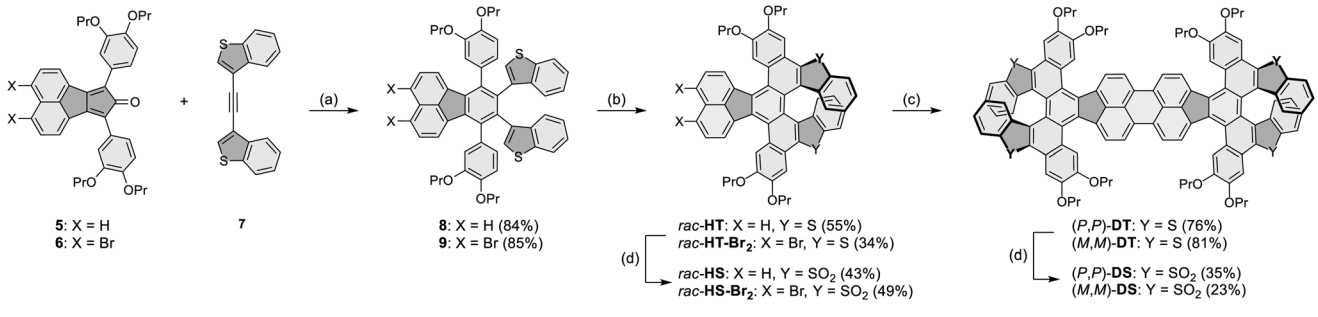

Fig. 2 Synthesis of diindenoperylene-embedded double dithia[7]helicene **DT** and double [7]helicenedisulfone **DS**, and of monohelicenes **HT**, **HT-Br$_2$**, **HS**, and **HS-Br$_2$**. (a) 200–220 °C, 14–18 h. (b) DDQ, TfOH, CH_2Cl_2, 0 °C, 30 min. (c) [Ni(COD)$_2$], COD, DMAP, THF, 60 °C, 2 h. (d) *m*-Chloroperoxybenzoic acid, CH_2Cl_2, 0 °C, 5–24 h. COD = 1,5-cyclooctadiene; DDQ = 2,3-dichloro-5,6-dicyano-1,4-benzoquinone; DMAP = 4-dimethylaminopyridine; Pr = *n*-propyl; THF = tetrahydrofuran; TfOH = trifluoromethanesulfonic acid.

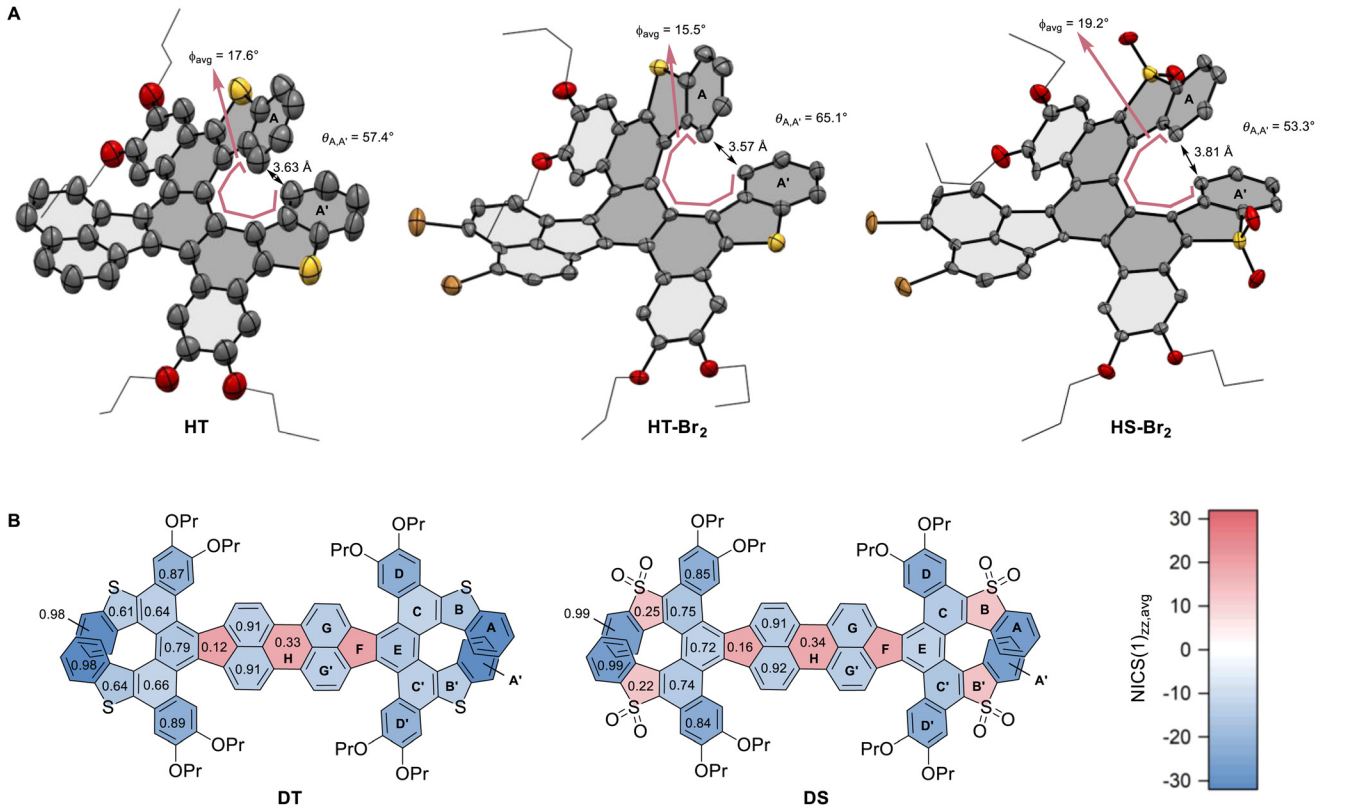

Fig. 3 (A) ORTEP representation of the single crystal X-ray structures of **HT**, **HT-Br$_2$**, and **HS-Br$_2$**. For clarity, hydrogen atoms are omitted and alkyl chains are represented as wireframes. Color code: (C: grey; O: red; S: yellow; Br: orange). Shown are average torsion angles of *cove* region C–C–C–C bonds (ϕ_{avg}), dihedral angles between terminal rings A, A′ ($\Theta_{A,A'}$), and helical pitch (for detailed definition, see the SI). (B) Calculated NICS(1)$_{zz,avg}$ (color coded) and HOMA (written) indices at the GIAO-CAM-B3LYP/def2-TZVP/D3BJ level of theory for compounds **DT** and **DS**.

Table 1 Aromaticity indices of thiophene units of the investigated helicenes. HOMA indices are derived from single crystal X-ray structures, unless noted otherwise. NICS(1)$_{zz,avg}$ values computed at the GIAO-CAM-B3LYP/def2-TZVP/D3BJ level of theory[44]

Compound	Avg. HOMA index of thiophene units	Avg. NICS(1)$_{zz,avg}$ index of thiophene units[b]
HT	0.55	−13.8
HT-Br$_2$	0.62	−13.9
HS	0.23[a]	11.3
HS-Br$_2$	−0.17	11.2
DT	0.63[a]	−13.8
DS	0.24[a]	11.2

[a] Computational geometry (CAM-B3LYP/def2-TZVP/D3BJ) was utilized. [b] For simplicity, average NICS(1)$_{zz,avg}$ of NICS(1)$_{zz}$ and NICS(−1)$_{zz}$ of all thiophene units in the molecules was calculated (for specific values, see the SI).

tional stability. In this study, the enantiomers were indeed successfully separated without special precautions using chiral HPLC and no indication of racemization was observed. To verify the configurational stability, the process of racemization was investigated computationally (r^{2}SCAN-3c,[45] SI) using **HT** as a model compound. The calculated C_s-symmetric transition state lies approximately 159 kJ mol^{-1} above the minima, consistent with negligible racemization and excellent configurational stability at rt. In contrast, the [5]helicene units, formed by rings D, C, E, F, G, and D', C', E, F, G', respectively, have a considerably lower calculated barrier of racemization of only 51 kJ mol^{-1}. The expected rapid interconversion under ambient conditions is consistent with the apparent C_2 symmetry in NMR studies. The heterochiral diastereomer of the [5]helicene units was found to be energetically favored over the homochiral diastereomer by 2 kJ mol^{-1}, consistent with the observed crystal structures.

Chiroptical and electrochemical properties

The optoelectronic and chiroptical properties of mono- and double helicenes are summarized in Fig. 4 and Table 2. The substitution and oxidation state of the monohelicenes impacts their UV/vis absorption properties (Fig. 4A). The bromination leads to a bathochromic shift of the lowest-energy absorption maximum from 493 nm (**HT**) to 513 nm (**HT-Br$_2$**) and from 513 nm (**HS**) to 526 nm (**HS-Br$_2$**). Oxidation of the sulfur atoms leads to red-shifts of 13 nm (**HS-Br$_2$** *vs.* **HT-Br$_2$**) or 20 nm (**HS** *vs.* **HT**), as well as an increase in the molar extinction coefficient of the lowest-energy absorption maximum (ε = 1.68 × 10^4 M^{-1} cm^{-1} (**HS-Br$_2$**) *vs.* 6.86 × 10^3 M^{-1} cm^{-1} (**HT-Br$_2$**); ε = 1.42 × 10^4 M^{-1} cm^{-1} (**HS**) *vs.* 8.11 × 10^3 M^{-1} cm^{-1} (**HT**)). Unsubstituted helicene **HT** shows fluorescence ($\lambda_{em,max}$ =

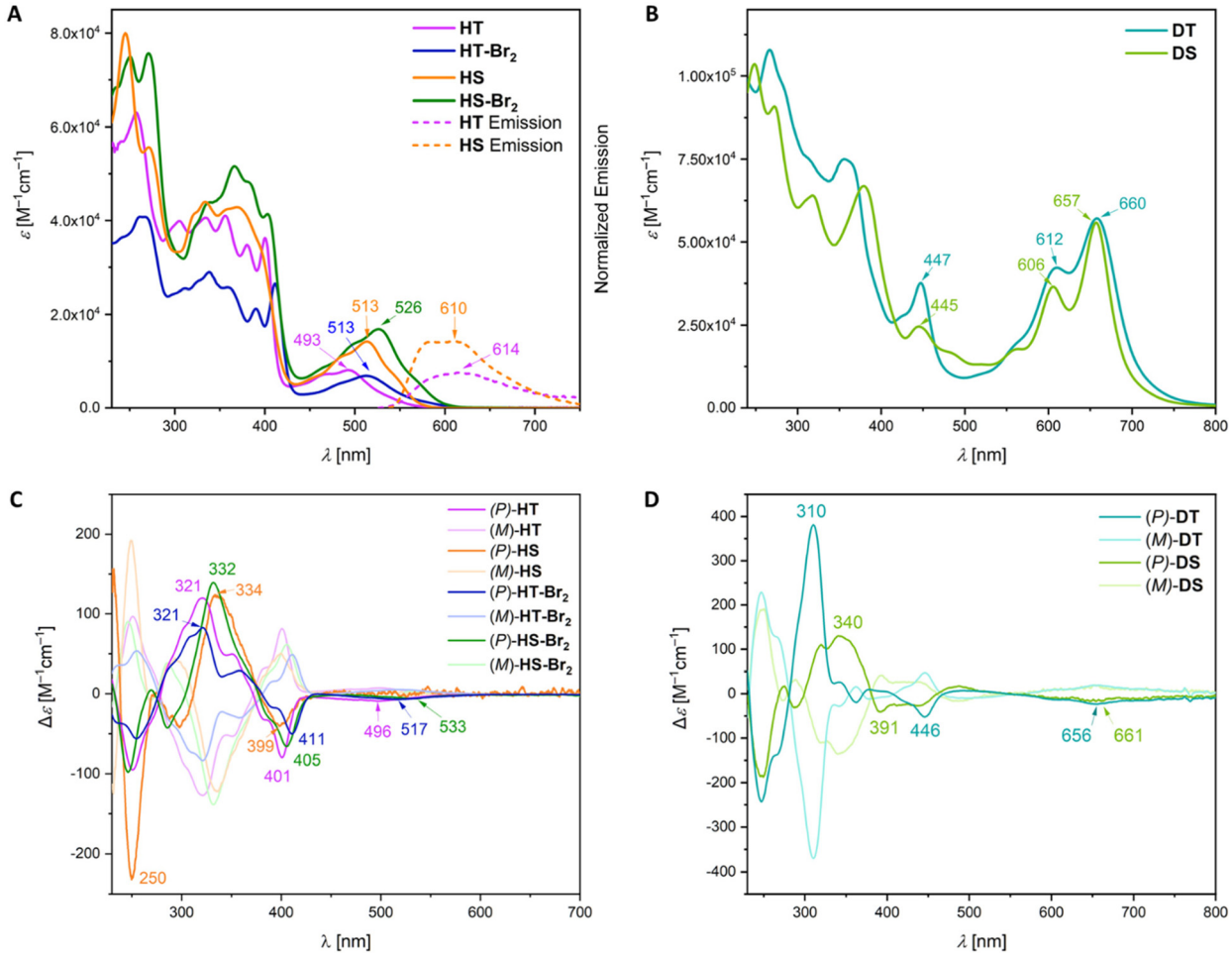

Fig. 4 UV/Vis absorption and emission spectra of monohelicenes (A) and double helicenes (B). CD spectra of monohelicenes (C) and double helicenes (D). All measurements in CH_2Cl_2, rt, approx. 10^{-5} M.

Table 2 Experimental optoelectronic, chiroptical, and electrochemical data of the title compounds. UV/Vis absorption and CD spectra recorded in CH_2Cl_2 at rt. Reduction and oxidation potentials were measured by cyclic voltammetry in CH_2Cl_2 at rt with *n*-Bu_4NPF_6 as the supporting electrolyte and are referenced *versus* Fc/Fc^+

Compound	λ_{max} [nm] ($\varepsilon(\lambda_{max})$ [M^{-1} cm^{-1}])	$\lambda_{\Delta\varepsilon_{max}}$ [nm] ($\Delta\varepsilon_{max}$ [M^{-1} cm^{-1}])	$\lambda_{g_{abs,max}}$ [nm] ($g_{abs,max}$)	$E_{red,1}$ [V]	$E_{ox,1}$ [V]
HT	493 (8.11×10^3)	332 (139)	331 (3.62×10^{-3})	−1.86	+0.52
HT-Br$_2$	513 (6.86×10^3)	321 (83.2)	321 (3.33×10^{-3})	−1.77	+0.58
HS	513 (1.42×10^4)	250 (212)	334 (2.80×10^{-3})	−1.37	+1.00
HS-Br$_2$	526 (1.68×10^4)	321 (123)	319 (3.26×10^{-3})	−1.34	+0.98
DT	660 (5.96×10^4)	310 (376)	311 (5.68×10^{-3})	−1.24	+0.44
DS	657 (5.58×10^4)	340 (132)	343 (2.13×10^{-3})	−1.01	+0.78

614 nm), albeit with a low quantum yield (1.9%). **HS** shows fluorescence at $\lambda_{em,max}$ = 610 nm with a higher quantum yield (9.0%). After dimerization to the perylene **DT**, the lowest-energy absorption maximum drastically shifts to 660 nm (ε = 5.69×10^4 M^{-1} cm^{-1}, Fig. 4B). Despite its oxidized thiophene units, **DS** shows nearly the same low-energy absorption bands ($\lambda_{abs,max}$ = 657 nm, ε = 5.58×10^4 M^{-1} cm^{-1}). Time-dependent density functional theory (TD-DFT) calculations (CAM-B3LYP (D3BJ)/def2-TZVP/SMD(CH_2Cl_2), for details, see the SI) indicate that the lowest-energy absorption band is dominated by a HOMO–LUMO transition, with both molecular orbitals being localized mostly on the diindenoperylene unit.

Neither **DT** nor **DS** shows any detectable photoluminescence between 600 and 1600 nm. In general, the extended structures comprising highly flexible [5]helicene units may facilitate non-radiative relaxation processes, outcompeting fluorescence.[46]

All enantiopure helicenes showed circular dichroism (CD) (Fig. 4C and D and Table 2). The absolute configurations were assigned based on TD-DFT (CAM-B3LYP(D3BJ)/def2-TZVP/SMD

(CH_2Cl_2)) simulated CD spectra (for details, see the SI). Out of the monomeric helicenes, the unsubstituted **HS** has the highest absolute $\Delta\varepsilon$ (212 M^{-1} cm^{-1} at 250 nm), while **HT**, **HT-Br$_2$** and **HS-Br$_2$** show their highest $\Delta\varepsilon$ in the range of 321 nm–332 nm. **HT** offers the highest $g_{abs,max}$ (3.62×10^{-3} at 331 nm). The double helicene **DT** shows even higher $\Delta\varepsilon$ (376 M^{-1} cm^{-1} at 310 nm) and $g_{abs,max}$ (5.68×10^{-3} at 311 nm), values significantly higher than those of **DS** ($\Delta\varepsilon$ = 132 M^{-1} cm^{-1} at 340 nm and $g_{abs,max}$ = 2.13×10^{-3} at 343 nm). These values are comparable to those reported for [6]helicene **1** ($g_{abs,max}$ = 1.5×10^{-3})[16] and double [6]helicene **2** (g_{abs} = 7.0×10^{-3}).[17]

The electrochemical properties of all compounds were investigated by cyclic voltammetry measurements in CH_2Cl_2 with n-Bu_4NPF_6 as the supporting electrolyte *versus* ferrocene/ferrocenium (*vs.* Fc/Fc^+). The redox potentials of the dimeric helicenes were impacted by oxidation of the thiophene units (Table 2 and Fig. 5). Sulfone **DS** is both oxidized and reduced at higher potentials than **DT** with the thiophene units. The anodic shift is in agreement with the electron-withdrawing nature of the sulfone moieties. Hence, the first oxidation is shifted by +340 mV (+0.44 V (**DT**) *vs.* +0.78 V (**DS**) (*vs.* Fc/Fc^+)) and the first reduction by +230 mV (−1.24 V (**DT**) *vs.* −1.01 V (**DS**)). In the monomeric helicenes **HT** and **HS**, the effect of oxidation of the thiophene units is even more pronounced. The first oxidation potential occurs anodically shifted by +480 mV (0.52 V (**HT**) *vs.* 1.00 V (**HS**)) and the first reduction by +490 mV (−1.86 V (**HT**) *vs.* −1.37 V (**HS**)). In contrast, the bromo substitution in the monomeric helicenes **HT-Br$_2$** and **HS-Br$_2$** has only a negligible impact on the redox potentials, all of which occur within a range of ±0.1 V compared to parent **HT** and **HS** (for details, see the SI). All discussed redox events for helicenes and double helicenes were reversible or quasi-reversible with the exception of **HT-Br$_2$**, where the reduction is irreversible (see the SI).

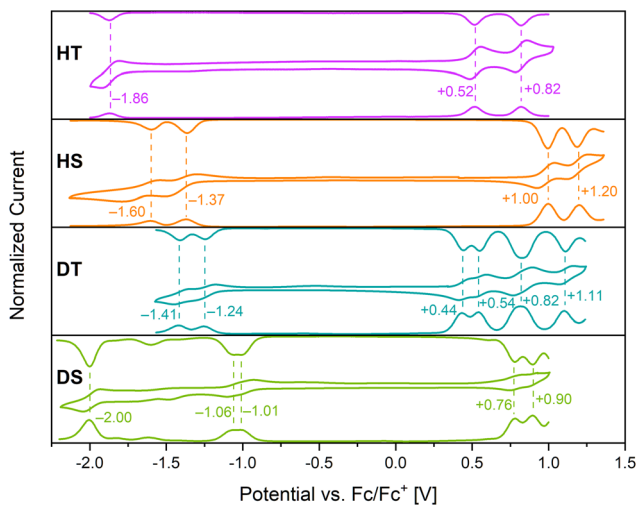

Fig. 5 Cyclic voltammetry (CV, middle), differential pulse voltammetry (DPV, top) and square wave voltammetry (SWV, bottom) measurements of single and double helicenes in CH_2Cl_2 at rt (approx. 2 mM, n-Bu_4NPF_6 as the supporting electrolyte, CV: scan rate 149 mV s^{-1}. DPV: step potential 20 mV, pulse width 50 ms, pulse period 200 ms, and pulse amplitude 50 mV. SWV: step potential 10 mV, square-wave amplitude 25 mV and square-wave frequency 15 Hz).

Conclusions

π-Extended double dithia[7]helicenes **DT** and **DS** with a diindenoperylene core were synthesized and investigated for their structural, chiroptical and electrochemical properties. Our newly developed synthetic route involving Diels–Alder and Scholl reactions followed by Yamamoto coupling as the key step provides versatile access to a broad range of functionalized helicenes. The oxidation of the thiophene units to the corresponding sulfone acceptors further modulates the photophysical and redox properties of the compounds. While no fluorescence was detected for both **DT** and **DS**, intense bathochromically shifted UV/vis absorption maxima up to 660 nm and considerable dissymmetry factors reaching 5.68×10^{-3} were observed for **DT**. Computational analysis revealed excellent configurational stability of the [7]helicene unit ($\Delta E^{\ddagger}$ = 159 kJ mol^{-1}), potentially enabling long-term applications of our π-extended [7]helicenes without risk of racemization.

Author contributions

The manuscript was written through contributions from all authors. All authors have given approval to the final version of the manuscript. Conceptualization: J. B. and M. K; methodology: G. B. and J. B.; investigation: G. B.; computational analysis: G. B.; X-ray crystallographic analysis: F. R.; writing – original draft: G. B.; writing – review and editing: J. B. and M. K.

Conflicts of interest

There are no conflicts to declare.

Data availability

The data supporting this article have been included as part of the supplementary information (SI). Supplementary information: synthetic and computational details and characterization data. See DOI: **https://doi.org/10.1039/d5qo01701g**.

CCDC 2516116–2516118 contain the supplementary crystallographic data for this paper.[47a–c]

Acknowledgements

The generous funding from Deutsche Forschungsgemeinschaft (DFG), project number 281029004-SFB 1249, is acknowledged. The authors acknowledge support from the State of Baden-Württemberg through bwHPC and the German Research Foundation (DFG) through grant no. INST 40/575-1 FUGG (JUSTUS 2 cluster).

References

1 M. Rickhaus, M. Mayor and M. Juríček, Chirality in Curved Polyaromatic Systems, *Chem. Soc. Rev.*, 2017, **46**, 1643.
2 J. R. Brandt, F. Salerno and M. J. Fuchter, The Added Value of Small-Molecule Chirality in Technological Applications, *Nat. Rev. Chem.*, 2017, **1**, 0045.
3 M. Rickhaus, M. Mayor and M. Juríček, Strain-Induced Helical Chirality in Polyaromatic Systems, *Chem. Soc. Rev.*, 2016, **45**, 1542.
4 B. P. Bloom, Y. Paltiel, R. Naaman and D. H. Waldeck, Chiral Induced Spin Selectivity, *Chem. Rev.*, 2024, **124**, 1950.
5 C. Thilgen and F. Diederich, Structural Aspects of Fullerene Chemistry – A Journey through Fullerene Chirality, *Chem. Rev.*, 2006, **106**, 5049.
6 H. V. Anderson, N. D. Gois and W. A. Chalifoux, New Advances in Chiral Nanographene Chemistry, *Org. Chem. Front.*, 2023, **10**, 4167.
7 J. M. Fernández-García, P. J. Evans, S. Filippone, M. Á Herranz and N. Martín, Chiral Molecular Carbon Nanostructures, *Acc. Chem. Res.*, 2019, **52**, 1565.
8 R. Gutierrez, E. Díaz, R. Naaman and G. Cuniberti, Spin-Selective Transport through Helical Molecular Systems, *Phys. Rev. B:Condens. Matter Mater. Phys.*, 2012, **85**, 081404(R).
9 Y. Yang, R. C. da Costa, M. J. Fuchter and A. J. Campbell, Circularly Polarized Light Detection by a Chiral Organic Semiconductor Transistor, *Nat. Photonics*, 2013, **7**, 634.
10 Y. Chen, Circularly Polarized Luminescence Based on Small Organic Fluorophores, *Mater. Today Chem.*, 2022, **23**, 100651.
11 O. G. Willis, F. Zinna and L. Di Bari, NIR-Circularly Polarized Luminescence from Chiral Complexes of Lanthanides and d-Metals, *Angew. Chem., Int. Ed.*, 2023, **62**, e202302358.
12 M. S. Newman and D. Lednicer, The Synthesis and Resolution of Hexahelicene, *J. Am. Chem. Soc.*, 1956, **78**, 4765.
13 J. Barroso, J. L. Cabellos, S. Pan, F. Murillo, X. Zarate, M. A. Fernandez-Herrera and G. Merino, Revisiting the Racemization Mechanism of Helicenes, *Chem. Commun.*, 2018, **54**, 188.
14 C. Goedicke and H. Stegemeyer, Resolution and Racemization of Pentahelicene, *Tetrahedron Lett.*, 1970, **11**, 937.
15 R. H. Martin and M.-J. Marchant, Thermal Racemisation of [6], [7], [8] and [9] Helicene, *Tetrahedron Lett.*, 1972, **13**, 3707.
16 N. J. Schuster, D. W. Paley, S. Jockusch, F. Ng, M. L. Steigerwald and C. Nuckolls, Electron Delocalization in Perylene Diimide Helicenes, *Angew. Chem., Int. Ed.*, 2016, **55**, 13519.
17 J.-K. Li, X.-Y. Chen, W.-L. Zhao, Y.-L. Guo, Y. Zhang, X.-C. Wang, A. C.-H. Sue, X.-Y. Cao, M. Li, C.-F. Chen and X.-Y. Wang, Synthesis of Highly Luminescent Chiral Nanographene, *Angew. Chem., Int. Ed.*, 2023, **62**, e202215367.
18 L. Zhou, H. Liu, J. Tan, C. Liu, X.-Y. Cao, A. Narita and Y. Hu, Double Thia/sulfone[7]helicenes with Controlled Photophysical and Chiroptical Properties by Heteroatom Variation, *Chem. – Asian J.*, 2022, **17**, e202200336.
19 A. Swain, F. Rominger and M. Mastalerz, C_2-Symmetric Perylene-Embedded Double [5]Helicenes, *Org. Lett.*, 2025, **27**, 8770.
20 Y. Xia, W. Sun, Q. Yang, L. Jiang, Y. Wang, Y. Hu and F. Chen, Saddle-Shaped Chiral Nanographenes Embedded with Dipleiadiene and Thia[6]helicene Units, *Org. Chem. Front.*, 2025, **12**, 6980.
21 L. M. Ramaniah and M. Boero, Structural, Electronic, and Optical Properties of the Diindenoperylene Molecule from First-Principles Density-Functional Theory, *Phys. Rev. A*, 2006, **74**, 042505.
22 V. M. Nichols, K. Broch, F. Schreiber and C. J. Bardeen, Excited-State Dynamics of Diindenoperylene in Liquid Solution and in Solid Films, *J. Phys. Chem. C*, 2015, **119**, 12856.
23 D. Kurrle and J. Pflaum, Exciton Diffusion Length in the Organic Semiconductor Diindenoperylene Available, *Appl. Phys. Lett.*, 2008, **92**, 133306.
24 K. Nogi and H. Yorimitsu, Aromatic Metamorphosis: Conversion of an Aromatic Skeleton into a Different Ring System, *Chem. Commun.*, 2017, **53**, 4055.
25 A. Kaga, H. Iida, S. Tsuchiya, H. Saito, K. Nakano and H. Yorimitsu, Aromatic Metamorphosis of Thiophenes by Means of Desulfurative Dilithiation, *Chem. – Eur. J.*, 2021, **27**, 4567.
26 M. Bhanuchandra, K. Murakami, D. Vasu, H. Yorimitsu and A. Osuka, Transition-Metal-Free Synthesis of Carbazoles and Indoles by an SNAr-Based "Aromatic Metamorphosis" of Thiaarenes, *Angew. Chem., Int. Ed.*, 2015, **54**, 10234.
27 K. Uematsu, C. Hayasaka, K. Takase, K. Noguchi and K. Nakano, Transformation of Thia[7]helicene to Aza[7] helicenes and [7]Helicene-like Compounds via Aromatic Metamorphosis, *Molecules*, 2022, **27**, 606.
28 J. Borstelmann, J. Bergner, F. Rominger and M. Kivala, A Negatively Curved π-Expanded Pyracylene Comprising a Tropylium Cation, *Angew. Chem., Int. Ed.*, 2023, **62**, e202312740.
29 S. H. Pun and Q. Miao, Introduction of Eight-Membered Rings to Polycyclic Arenes by Ring Expansion, *Chin. J. Org. Chem.*, 2020, **40**, 3347.
30 J. Kruszewski and T. M. Krygowski, Definition of Aromaticity Basing on the Harmonic Oscillator Model, *Tetrahedron Lett.*, 1972, **13**, 3839.
31 J. C. Dobrowolski and S. Ostrowski, HOMA Index Establishes Similarity to a Reference Molecule, *J. Chem. Inf. Model.*, 2023, **63**, 7744.
32 J. R. Cheeseman, G. W. Trucks, T. A. Keith and M. J. Frisch, A Comparison of Models for Calculating Nuclear Magnetic Resonance Shielding Tensors, *J. Chem. Phys.*, 1996, **104**, 5497.
33 R. Ditchfield, Self-Consistent Perturbation Theory of Diamagnetism, *Mol. Phys.*, 1974, **27**, 789.

34 T. A. Keith and R. F. W. Bader, Calculation of Magnetic Response Properties Using Atoms in Molecules, *Chem. Phys. Lett.*, 1992, **194**, 1.
35 K. Wolinski, J. F. Hinton and P. Pulay, Efficient Implementation of the Gauge-Independent Atomic Orbital Method for NMR Chemical Shift Calculations, *J. Am. Chem. Soc.*, 1990, **112**, 8251.
36 R. McWeeny, Perturbation Theory for the Fock-Dirac Density Matrix, *Phys. Rev.*, 1962, **126**, 1028.
37 F. London, Théorie quantique des courants interatomiques dans les combinaisons aromatiques, *J. Phys. Radium*, 1937, **8**, 397.
38 T. A. Keith and R. F. W. Bader, Calculation of Magnetic Response Properties Using a Continuous Set of Gauge Transformations, *Chem. Phys. Lett.*, 1993, **210**, 223.
39 T. Yanai, D. P. Tew and N. C. Handy, A New Hybrid Exchange–Correlation Functional Using the Coulomb-Attenuating Method (CAM-B3LYP), *Chem. Phys. Lett.*, 2004, **393**, 51.
40 S. Grimme, S. Ehrlich and L. Goerigk, Effect of the Damping Function in Dispersion Corrected Density Functional Theory, *J. Comput. Chem.*, 2011, **32**, 1456.
41 A. Schäfer, C. Huber and R. Ahlrichs, Fully Optimized Contracted Gaussian Basis Sets of Triple Zeta Valence Quality for Atoms Li to Kr, *J. Chem. Phys.*, 1994, **100**, 5829.
42 F. Weigend and R. Ahlrichs, Balanced Basis Sets of Split Valence, Triple Zeta Valence and Quadruple Zeta Valence Quality for H to Rn: Design and Assessment of Accuracy, *Phys. Chem. Chem. Phys.*, 2005, **7**, 3297.
43 M. Garcia-Ratés and F. Neese, Effect of the Solute Cavity on the Solvation Energy and its Derivatives within the Framework of the Gaussian Charge Scheme, *J. Comput. Chem.*, 2020, **41**, 922.
44 Z. Wang, py.Aroma: An Intuitive Graphical User Interface for Diverse Aromaticity Analyses, *Chemistry*, 2024, **6**, 1692.
45 S. Grimme, A. Hansen, S. Ehlert and J.-M. Mewes, r^{2}SCAN-3c: A "Swiss Army Knife" Composite Electronic-Structure Method, *J. Chem. Phys.*, 2021, **154**, 64103.
46 T. Iimori, T. Ishikawa, Y. Torii, H. Tamaya, H. Nakano and M. Kanno, Effect of Rigidity of Microenvironment on Fluorescence of 7,7,8,8-Tetracyanoquinodimethane (TCNQ), *Chem. Phys. Lett.*, 2020, **738**, 136912.
47 (*a*) CCDC 2516116: Experimental Crystal Structure Determination, 2026, DOI: **10.5517/ccdc.csd.cc2qg71h**; (*b*) CCDC 2516117: Experimental Crystal Structure Determination, 2026, DOI: **10.5517/ccdc.csd.cc2qg72j**; (*c*) CCDC 2516118: Experimental Crystal Structure Determination, 2026, DOI: **10.5517/ccdc.csd.cc2qg73k**.